Bearing capacity assessment of a XIV century arch bridge in Lecco (Italy)

Paolo Martinelli[1*], Andrea Galli[1], Luigi Barazzetti[2], Matteo Colombo[1], Roberto Felicetti[3], Mattia Previtali[4], Fabio Roncoroni[5], Marcello Scola[6] and Marco di Prisco[7]

[1] Assistant Professor, Politecnico di Milano, Department of Civil and Environmental Engineering, P.za L. da Vinci 32, 20133 Milan (Italy).

[*] Corresponding author, e-mail: paolo.martinelli@polimi.it; tel: 0039-0223998785; fax: 0039-0223998771

[2] Assistant Professor, Politecnico di Milano, Department of Architecture, Built environment and Construction engineering, Via Ponzio 31, 20133 Milan (Italy).

[3] Associate Professor, Politecnico di Milano, Department of Civil and Environmental Engineering, P.za L. da Vinci 32, 20133 Milan (Italy).

[4] Temporary researcher, Politecnico di Milano, Department of Architecture, Built environment and Construction engineering, Via Ponzio 31, 20133 Milan (Italy).

[5] Senior Engineer, Politecnico di Milano, Polo Territoriale di Lecco, via Previati 1/c, 23900 Lecco (Italy).

[6] Senior Engineer, Politecnico di Milano, Department of Civil and Environmental Engineering, P.za L. da Vinci 32, 20133 Milan (Italy).

[7] Professor, Politecnico di Milano, Department of Civil and Environmental Engineering, P.za L. da Vinci 32, 20133 Milan (Italy).

ABSTRACT

The paper presents the results of an experimental and numerical investigation on Azzone Visconti bridge, a XIV century arch bridge in Lecco (northern Italy). Starting from the historical data and from an extensive mechanical characterization of both the soil constituting the riverbed and of the masonry constituting the piers, the aim of the study is to investigate the bearing capacity of the bridge. A testing loading scheme defined according to the current Italian Code is adopted to check the structural behaviour. A simplified finite element structural model was conceived and calibrated as a control tool to safely perform the experimental tests. Post-test nonlinear finite element analyses have allowed the prediction of the bridge bearing capacity and the definition of the bridge class according to the Italian regulations.

Keywords: Masonry arch bridge; 3D geometrical survey; non-destructive tests; cored sample tests; on-site bearing load test; numerical FE analyses; soil-structure interaction

1 INTRODUCTION

The structural safety and conservation of historical structures belonging to the cultural heritage is a prominent concern in our society. This issue becomes a main issue in Italy, which hosts the largest amount of historical churches, monasteries, and towers in the world as well as the largest number of UNESCO world heritage sites (UNESCO World Heritage List, 2017). Historical bridges are an important part of a country architectural heritage. Only the Lombardy region (with about 10 million people constitutes one-sixth of Italy's population) counts 85 bridges classified as protected architectural heritage (Lombardia Beni Culturali, 2017).

Historical bridges are fragile structures exposed to damaged deriving from several causes: beyond the effect of the applied working loads, among the possible other causes it is worth remembering the pollution effects, the presence of vegetation, the action of water currents, the occurrence of natural hazards such as seismicity, flooding or others (Perez-Gracia, 2011). The increase in vehicular traffic, as well as the increase in the maximum permissible accidental loads, represents additional possible factors of damage for the structure. To guarantee safe working conditions, the bridges bearing capacity must be assessed and their demand levels should be carefully assigned.

The assessment of historical bridges was traditionally carried out by means of a simple visual inspection (see e.g. O'Connor, 1994; Ural et al., 2008), in some cases supported by non-destructive techniques. However, owing to the complex structural behaviour of historical arch bridges, destructive testing on small material portions extracted from the structure as well as on-site tests are often an unavoidable part of the assessment procedure, allowing meaningful estimations of the mechanical characteristics of the structure.

Empirical, analytical and numerical approaches also represent a precious tool to assess

the load carrying capacity of masonry bridges. To this regards, several approaches have been proposed in the literature, ranging from expeditious procedures such empirical methods (UK Department of Transports, 1997), through limit analysis methods (Heyman, 1982; Harvey, 1988; Gilbert and Melbourne, 1994) to complex refined methods as the distinct element method (Lemos, 2007) or the finite element (FE) method. In the latter case, either one-dimensional (Molins and Roca, 1998; Boothby, 2001; Brencich and De Francesco, 2004; de Felice, 2009, De Santis and de Felice, 2014), two-dimensional or three-dimensional elements (Fanning and Boothby, 2001; Cavicchi and Gambarotta, 2005; Milani and Lourenço, 2012) can be adopted.

The present paper focuses the attention on the Azzone Visconti bridge, a masonry arch bridge which has been for centuries (until 1955) the unique road connection between the two banks of Adda river, the only emissary of Lake Como, and it has still been an important access road to the town of Lecco (northern Italy) up to 2014 when the assessment activities started. The bridge, built in the XIV century, is even the most important medieval testimony present in the city, and it is one of the most impressive masonry work of the entire region. The structure, therefore, has a great importance for its historical value, being also one of the 85 bridges classified as protected architectural heritage of the Lombardy region. An authoritative source (Magnani, 2014) has recently supposed that it corresponds to the bridge in the background of the famous Mona Lisa masterpiece of Leonardo da Vinci.

The construction of other two bridges in the proximity of Azzone Visconti bridge (Kennedy bridge built in 1955 and, later, the Manzoni bridge opened in 1985) has significantly reduced the vehicle traffic on the bridge.

Within the framework of an institutional collaboration between Politecnico di Milano

(Polo Territoriale di Lecco) and the Municipality of Lecco (Italy), an extensive research activity involving several disciplines and research groups has been initiated in 2014, with the aim of investigating the bearing capacity of the bridge, under the scientific coordination of the last author.

2 BRIDGE HISTORY AND PAST STRENGTHENING INTERVENTIONS

The Azzone Visconti bridge (also known as "Ponte Vecchio") is a historical masonry arch bridge built in the XIV century consisting of ten piers, eleven arches and two bridge abutments, one on the Lecco side (left side) and one on the Malgrate side (right side) of the Adda river. During its life, the bridge experienced several modifications of length and use, hosting even (for a certain period) a military fortress with a drawbridge (Figs. 1a-b). Although the bridge appears today very different from the original construction, it remains one of the most important testimonies of military engineering of the middle age, besides being explicitly mentioned in the novel *The Betrothed* by Alessandro Manzoni (in Italian *I promessi sposi*), set during Spanish domination.

The bridge was realized by the wish of the Lord of Milan, Azzone Visconti, between 1336 and 1338, connecting for the first time in the territory the two sides of the Adda river, which had belonged until then to the Duchy of Milan and to the Republic of Venice. Originally equipped with Medieval war machines (i.e. large crossbow), it served as a funnel for the access of men and goods to the village of Lecco and from there to the German regions, guaranteeing its military protection. In the 17th century the defensive structure represented a customs instrument on the transit of goods.

The Azzone Visconti Bridge was originally built with eight arches. The bridge was later expanded into two steps (1350 and 1434) up to 11 arches to enlarge the river cross section favouring a faster water outflow in order to reduce the flooding of Como area.

The last two arches on the right side (connecting to Milan) were demolished in 1800 during the Franco-Austrian conflict (Fig. 1c).

At the beginning of the XX century (1909-1910), the existing deck (Fig. 1d) was enlarged using cantilever steel members to host a tramway (Fig. 1e).

In 1949-1950, in order to facilitate the outflow of the river, the riverbed was reduced of about two meters. To protect the bridge piers, strengthening works were carried out on the foundations of 7 piers (Figs. 2a-c). During the design phase some geognostic surveys were carried out in the riverbed. The foundations of each pier were reinforced by introducing a large diameter steel encasing ring, about five meters deep, filled by concrete and constrained at the top by an additional external reinforced concrete ring (Fig. 2a-c).

In 1959 important strengthening interventions were realized due to the deterioration of the metallic members added in 1909-1910 and in view of the need to enlarge the roadway. In particular, the deck was completely removed (Fig. 2d) and a continuous concrete caisson (Fig. 2e-f) was inserted between the north and south masonry spandrel walls and filled with coarse granular material (mix of pebbles and mortar). Three arches damaged by the out of plums of the piers were also strengthened (Fig. 2e). External pedestrian footbridges were also added using cantilever steel beams and RC slabs resting on the aforementioned steel beams. No further interventions were carried out in the last fifty years, with only an ordinary maintenance activity.

Nevertheless, there has been a significant deterioration of the cantilever steel beams located at a distance of 4 m orthogonally to the longitudinal axis of the bridge and of the reinforcements of the slabs that constituted the pedestrian platform of the sidewalks. In 2013, the observation of the aforementioned damages led the Municipality to close the sidewalks.

The width of the deck therefore varies from 6.3 m to 6.75 m. In the current investigations, the attention will be not devoted on the state of degradation of the top RC slab in which the steel profiles are embedded. The latter are seriously oxidized and their flexural capacity is irremediably compromised. A picture of the bridge as it appears nowadays is shown in Figure 1f.

3 3D SURVEY OF THE BRIDGE GEOMETRY

A survey campaign was carried out to detect the bridge geometry and to support the generation of the FE model. In particular, three survey strategies were combined:

- a geodetic network to provide a robust reference system for laser scanning and photogrammetric survey (Fig. 3a);
- a laser scanning survey to capture the irregular shape of the bridge (Fig. 3b);
- a photogrammetric survey to support definition of material characterization and material degradation (Fig. 3c).

A local reference system was established by means of a geodetic network. The network is made up of 6 stations and the measurement phase took one day. A total amount of 834 observations and 264 unknowns gave 570 degrees of freedom. Least Squares adjustment provided an average point precision of about ±1.5 mm.

To capture the complexity and the size of the bridge 77 scans were required, which were registered with the use of the established geodetic network. The instrument used is a Faro Focus 3D and the final point cloud is made up of 2.5 billion points. The instrument was set up in different positions, including the road and the riverbanks. During the processing phase scans were registered with an average precision of ±3 mm by using checkerboard targets measured with the total station and additional scan-to-scan correspondence (spherical targets).

Finally, a photogrammetric survey was carried out for the two elevations of the bridge (South and North), of the piers and of the vaulted surfaces (intrados) of the bridge span. In particular, the orthophotos of the two bridge elevations were generated by acquiring more than 500 images captured from a boat. Images were oriented via bundle adjustment and then orthophotos were generated. They were used in different stages of the project, for instance for planning the location of destructive and non-destructive analysis and for a complete stratigraphic analysis. The plan and front views of the bridge together with its main geometric properties are shown in Figure 4.

4 STRUCTURAL AND GEOTHECNICAL CHARACTERIZATION

4.1 Geotechnical characterization of the riverbed

With the aim of characterizing as precisely as possible the soil below the foundations of the bridge, a quite extensive on-site investigation campaign was carried out, in order to define a suitable geotechnical model for the whole riverbed. A common geognostic investigation techniques was adopted. This choice allowed to respect the limited budget, the reduced periods of traffic closure imposed by the Municipality and the severe constraints required by the Historical Authority.

One vertical core (external diameter equal to 127 mm; diameter of the sample equal to 101 mm) was drilled in piers 6, 7, 8, 9 and 10 (labelled G06 to G10, respectively; Fig. 4), in order to get a direct inspection of the internal filling of the piers and to investigate even the underlying riverbed. In particular, in piers 6, 8 and 10 continuous soil cores have been performed down to 27, 24 and 18 meters below the bridge deck, respectively. During coring, several (disturbed) soil samples were extracted, in order to derive the local grain size distribution. Dynamic penetrometric tests (SPT) were also performed at different depths below the deck (a modified SPT test was run, by employing a closed cone tip, with

a diameter of 51 mm and a cone angle of 60°). As an example, a view of the soil cores extracted below pier 8 between 15 and 18 meters depth is shown in Figure 5a, whilst the grain size distributions of seven soil samples extracted below the pier 8 are shown in Figure 5b (the depths are indicated in the labels of the curves). As it can be observed, the soil is essentially composed of sand and gravel, with some thin layers of silty sand. As an example, for pier 8, the SPT test run at 12 m depth gave 17/22/30 (expressed as blows number per 15 cm advancement of the cone tip), at 15 m gave 10/13/6, at 18 m gave 26/45/50, at 21 m 6/5/5 and at 24 m gave 9/15/35.

In piers 7 and 9 no soil coring were performed below the piers, but continuous dynamic penetrometric test (SPT-DPSH) were executed starting from the base of the pier, down to approximately 26 meters below the deck (the results are reported in Fig. 6). For the other five piers no direct investigations have been allowed by the authority, and only some old soil sampling (executed in 1941, and without any quantitative soil characterization) were available for piers 3 and 4. For the sake of completeness, they have been qualitatively considered in the definition of the geotechnical model of the riverbed (Fig. 6). Several layers of soils were recognized by direct inspection of the extracted cores, ranging from gravel, to silty sand, to silty clay. Despite this large variability, all the foundations of the piers are stably positioned into a layer of a rather uniform gravelly sand (or fine gravel), approximately 9 meters thick. The whole set of penetrometric data were then interpreted by means of the well-known abacuses proposed by Gibbs and Holtz (1957) and Bazaraa (1967), in order to estimate the relative density of the granular deposits. The correlations proposed by Schmertmann (1976) have finally allowed to derive representative profiles of the values of the friction angle. For the sake of simplicity (and always being on the safe side) a homogeneous soil characterization was assumed (relative density DR ≈ 30%;

effective friction angle ϕ' = 35°), corresponding with a mid-loose granular material. When not specified, the saturated unit weight of the soil was assumed to be equal to γ_{sat} = 18 kN/m^3.

4.2 Mechanical characterization of the piers

Sonic tests were carried out on piers 2, 3, 6, 7 and 8 with the aim of investigating the mechanical characteristics and the stratigraphy of the piers in their lower part.

The propagation of elastic waves in the masonry depends on the masonry texture and on the state of the damage. In particular, when the masonry has discontinuities (cracks, gaps, etc.), the propagation velocity of the waves decreases, because the medium is less dense.

Direct sonic tests were performed according to a regular mesh grid: 3 rows and 15 columns with distances between them approximately of 40 cm (see Fig. 7). The lowest row is about 100 cm from the basement, while the columns were extended to almost the full width of the pier starting (ending) at 30 cm from the rostrum (except in the pier 8 where the grid is extended to the total width of the pier).

Figure 7 shows surface graphs that associate the sonic velocity values to the whole area investigated by the test, based on a linear interpolation of the values calculated at each test point. This provides a velocity map that highlights areas with higher internal discontinuities.

The average velocities detected on the piers are typical of a good quality stone masonry. The velocity distribution is fairly uniform (also for the high thickness of the piers, equal to approximately 2.6 m). No remarkable cavities or discontinuities can be observed. Pier 2 is characterized by higher velocities compared to the other piers indicating higher density due to less voids perhaps reduced by mortar injection.

From the vertical cores G06 and G09 13 cylindrical specimens were extracted (diameter *D* equal to 80 mm) at depths ranging between 1.5 m to 10.6 m from the deck. Six specimens are constituted by homogeneous rock, whilst seven specimens are made by mixed pebbles and mortar. An average density of 2420 kg/m^3 was estimated for the samples. All the specimens were analysed by means of ultrasonic direct test (Bungey et al. 2006), and an average ultrasonic velocity of to 3.95 km/s was measured. Seven cylindrical specimens (80 mm height (*H*); aspect ratio *H/D* = 1) were tested under uniaxial compression test (CEN 12390-3, 2009), whilst the remaining six (with height H of about 40 mm; H/D=0.5) were tested under indirect tension test (Brazilian test; CEN 12390-6, 2009). Compression tests on homogeneous material provided strength values in the range of 50-150 MPa, while specimens composed by mixed pebbles and mortar provide values around 20 MPa; Brazilian tests gave an average tensile strength equal to 3.5 MPa with a coefficient of variation (COV) of 0.67.

Three horizontal cores were also carried out up for a length of 180 cm (diameter 50 mm) for piers 2, 6 and 7. The holes were then inspected by means of videoendoscopy. The processing of the videos captured during the videoendoscopies allowed the creation of a complete photograph of the inner surface of the hole. As an example, the results for pier 2 are shown in Figure 8. Twelve samples extracted from the horizontal cores allowed the execution of uniaxial compression (8 specimens) and indirect tensile tests (4 specimens) for the mechanical characterization of the stone used for the construction of the piers. Compression tests provided an average strength of 138 MPa (COV = 0.63), whilst Brazilian tests gave an average tensile strength equal to 16.3 MPa (COV = 0.19).

5 LOAD TESTS

5.1 Loading schemes

The load tests were designed looking to the provisions of the Italian Technical Regulations for Construction (NTC08, 2008), for a first class bridge. Although the clear width currently available on the bridge is approximately 5.25 m (distance between the two side guardrails), two loading lanes were provided with the perspective to restore the previous width.

Two types of test protocol were executed:

- Type A test: application of about 750 kN by means of truck mixers on arches 2, 4, 5, 6, 7, 8, 10 and 11;
- Type B test: application of about 1200 kN by means of truck mixers and steel coils on arch 7.

Type A test was realized by one or two four-axes truck mixers positioned at the centre of the roadway as schematically indicated in Figures 9a and 9d.

The most severe loading procedure (type B test) was carried out by step-wise positioning two sets of steel coils supported by a suitable steel frame and two four-axes truck mixers on the arch between piers 6 and 7 (Figs. 9b-9d). The truck mixers were positioned along a lane as prescribed by the Italian code (NTC08, 2008). Due to the reduced clear width of the bridge, the loads on the second lane were applied by means of steel coils resting on the frame and moved by a crane as shown schematically in Figure 9b-c. Four loading steps were considered (Fig. 9d).

Details on the test protocol for both test types A and B are given in Table 1. For type A test, the final letters "_1" and "_2" describe, respectively, a non-symmetrical and a symmetrical load scheme with respect to the keystone of the loaded arch, due to the

presence of one or two vehicles.

Figure 10a shows the 4 steel coils located close to the side guard-rails of the bridge deck (B2 load test). Figure 10b refers to the loading test B3, where a truck mixer is placed next to the four coils. Figures 10c and 10d show the arrangement of 4 coils and two truck mixers for the load test B4.

5.2 Displacement measurement technique

A geometric levelling was established to monitor vertical movements of the bridge during its testing phase. An optical level Zeiss Ni1 and a set of 6 levelling rods were employed to determine the deformation of the bridge. The instrument is equipped with a compensator and it creates a horizontal line of sight; levelling rods must have a regular graduation to obtain the scale of the levelled differences. According to the basic principle of levelling, the difference between two readings is the elevation difference between the two benchmarks. The process is repeated to obtain the height difference between backsight and foresight points. The total height difference between widely separated points can be measured by combining the progressive height differences. A benchmark is considered fixed, if it is connected to the structure so that it follows its movement. The displacement between points can be finally computed by measuring their difference of height in different epochs, e.g. before the test and during the bridge loading, with a simple difference of coordinates. Absolute displacements are determined by using as reference a benchmark located in a stable position, i.e. a position not affected by displacements during the loading test.

In the case of the bridge, the use of an optical level with the parallel plate glass micrometers gave the opportunity to improve reading precision. Rods with 5 mm graduations were employed, for which the collimation of the nearest reading with an

adjustment screw is directly connected to the displacement measured by a micrometer. This provides readings with a precision of ±0.05 mm, that are then estimated to ±0.005 mm by the operator.

The monitoring project of the bridge was carried out with 47 benchmarks. The final scheme for the bridge is illustrated in Figure 11. The design of an appropriate measurement scheme coupled with precise measurements allows the estimation of heights (and height variations for data taken at different epochs) with sub-millimeter precision. The design of optimal acquisition networks has a direct impact on the precision and reliability: series of closed loops with common points must be preferred to (i) improve the accuracy and (ii) obtain an immediate check based on misclosures. The adjustment of the network was carried out via least squares. Indicating with H_i the height of the backsight point and H_j the height of the foresight points, the observation equations for the levelling are in the form:

$$H_j - H_i = \Delta_{i,j} \quad (1)$$

Representing all the observations into a matrix form, it is possible to express the problem in the linear form:

$$\mathbf{Ax} = \mathbf{b} + \mathbf{v} \quad (2)$$

where $\boldsymbol{A}$ is the so called design matrix, $\boldsymbol{x}$ is the vector of the unknowns (i.e. heights of the benchmarks), $\boldsymbol{b}$ contains the observations, and $\boldsymbol{v}$ is the residual vector. In particular, the design matrix $\boldsymbol{A}$ made up of zeros and ±1 in correspondence of position i and j. The solution is:

$$\mathbf{x} = (\mathbf{A}^T\mathbf{A})^{-1}\mathbf{A}^T\mathbf{b} \quad (3)$$

As can be seen, no weight matrix was included in the adjustment. Indeed, the same set of level and rods was used for all the readings at different epochs and benchmarks are

regularly spaced. Finally, the covariance matrix of parameters can be estimated as

$$\mathbf{C_{xx}} = \sigma_0^2(\mathbf{A}^T\mathbf{A})^{-1} \quad (4)$$

where $\sigma_0^2 = \mathbf{v}^T\mathbf{v}/(n-m)$, in which *m* is the number of equations and *n* is the number of unknowns.

The precision of heights (after least squares adjustment) was about ±0.15 mm for all tests carried out with different load conditions. Points 10000, 2000 and 3000 were assumed as fixed benchmark, because they are outside the bridge.

6 FE NUMERICAL MODELS

In this section, two FE models are presented. The first is a predictive model developed in a pre-test phase, whose main purpose was to provide real time indications during the experimental test (service condition, SLS model). The latter is a nonlinear model developed after the bridge test whose purpose is to provide indications on the bearing capacity of the bridge (ULS model).

6.1 SLS model

6.1.1 Geometrical and material modelling

A bi-dimensional FE model of the whole bridge was created by means of the software Abaqus Standard 6.14 (2016). The main geometrical characteristics of the structure were derived from the topographical survey. The FE model combines several types of plane elements for different parts of the bridge as schematically indicated in Figure 12.

The piers and the filling material above the piers were discretized by employing plane stress elements (element type CPS3, three nodes with 2 DOFs per node and one integration point), whilst the vaults and the top RC caisson were modelled with beam elements (element type B21, two nodes and 3 DOFs per node). The top RC caisson was

connected to the underlying elements by means of equivalent springs (see Fig. 12). These latter were calibrated in order to reproduce the vertical deformability of the caisson, of the spandrel walls and internal filling. The upper limit over the piers modelled with plane stress elements corresponds to the depth of intervention of the strengthening works executed in 1959 (red line in Fig. 12). No tangential slip was allowed between top RC slab and the underlying elements. The vaults were rigidly connected to the piers (see point 6 of Fig. 12).

To ensure compatibility between beam elements and plane stress elements characterized by 3 and 2 degrees of freedom per node, the connection between the end of the arch (impost) and the pier was obtained via a "Multi-Point-Constraint" (Abaqus Standard 6.14, 2016). The connection with riverbed was modelled by means of two generalized spring elements, acting in series, whose constitutive model was carefully calibrated in order to reproduce mechanical behaviour of the soil within the encasing ring and of the underlying soil, respectively (see in the Section 6.1.2 for further details). The FE model is made by 6544 elements, 5384 of which are plane stress elements and 1160 are beam elements, and 4272 nodes.

A linear elastic mechanical behaviour for all the aforementioned components was assumed, since the loading scheme was not expected to induce significant nonlinear effects in the structure (service condition).

The experimental evidence and the historical data suggested to gather the piers into four homogeneous groups from the point of view of the mechanical characteristics. This differentiation was introduced into the finite element model as follows: (a) piers 1 and 2, (b) piers 3-7, (c) piers 8 and 9 and (d) pier 10. The main elastic characteristics of the materials adopted in the FE model are summarized in Table 2.

6.1.2 Derivation of the vertical equivalent stiffness

In the FE model the upper RC slab was assumed to work mainly in bending, whilst the underlying elements (masonry spandrel walls and granular filling material), serving as a support for the slab, to work mainly in compression. The latter are discretized as linear elastic springs in the FE model, whose stiffnesses k_e^A (or k_e^B depending on the load test cases) are computed as described in the following. For the sake of simplicity, the thickness of the filling material was assumed equal to the depth of the spandrel walls.

With reference to the cross-section of the bridge, the two load test situations (A, B) were considered (Fig. 13 shows type B test as an example). The deformability depends on the depth *h(x)* of the spandrel wall, that varies along the longitudinal development of the bridge (x-axis). Vertical stiffness is evaluated considering a unit longitudinal deck development, and it depends on the transverse load position and of the measurement points. The value $k_e^{A(B)}$ therefore is computed as the load applied divided by the displacement of the point considered for the measurements.

In Figure 13 the simplified scheme adopted for the definition of the equivalent axial stiffness is indicated. The scheme considers the upper RC beam supported at the ends on elastic constraints with stiffness k_m representing the spandrel wall, whereas the filling material acts as elastic soil with stiffness k_t playing the role of an elastic Winkler constant. For the sake of simplicity, the contribution of the RC wall inserted in 1959 to consolidate the masonry spandrel wall is neglected in the calculation.

Since the depth h of the spandrel wall varies along the longitudinal axis of the bridge, both k_m and k_t depend on the depth h. The stiffness k_m is expressed as:

$$k_m = \frac{E_m A}{h(x)} \tag{5}$$

where E_m represents the Young modulus of the spandrel wall assumed equal to E_m = 16

GPa, while A is the cross-section of the spandrel wall.

The Winkler constant k_t depends on the Young modulus of the filling material E_r assuming that the whole volume of material inside the caisson is in oedometric condition:

$$k_t = \frac{E_r}{h} \tag{6}$$

The Young modulus E_r is approximately calculated through the following empirical relationship, which is able to take into account the increase in the confining effect with the depth below the deck:

$$E_r = k\, p_a \left(\frac{p}{p_a}\right)^n \tag{7}$$

In Equation (7) p represents the mean component of the current geostatic pressure, p_a is the atmospheric pressure (p_a = 101325 Pa), k and n are two dimensionless constitutive parameters. These latter were calibrated on the basis of experimental data obtained by performing oedometric tests on granular material and taken respectively equal to k = 220, n = 0.22 (di Prisco and Galli, 2011). A representative vertical stress σ_v at depth $h/2$ under the deck, required for calculating the mean pressure p, is calculated as:

$$\sigma_v = \frac{1}{2} h\gamma \tag{8}$$

where γ is the unit weight of the filling material (assumed equal to 20 kN/m^3). Then, the estimated confinement pressure results equal to:

$$p = (1 + 2k_0)\frac{\sigma_v}{3} \tag{9}$$

where k_0 is the "at rest" earth pressure coefficient, assumed to be equal to 0.5.

6.1.3 Mechanical behaviour of the foundations

In the numerical analyses, for the sake of simplicity, the foundations of the piers were considered as isolated elements, i.e. any possible interaction or interference between

neighbour piers was disregarded. The authors are aware that this is a very rough simplifying hypothesis (it actually implies the loss of continuity in the soil), but it can be reasonably accepted, given that (i) in literature there no exist any exact formulation accounting such interaction, and (ii) any numerical evaluation (e.g. by means of preliminary FE simulations, modelling the whole riverbed as a continuum) would have required a much higher accuracy in the calibration of the soil constitutive models, than that it can be obtained by interpreting the results of the in situ test campaign. Moreover, (iii) the relatively small loading increment reached during the tests (less than 10% of self-weight of each pier) should not imply, in principle, any interaction mechanism to be activated. From a mechanical point of view, it is important to highlight that for this type of bridge the main contribution to the total expected vertical settlement is given by the soil deformability, rather than by piers of deck deformations. In order to correctly capture this aspect, the most appropriate models have to be implemented for the soil, but without introducing excessive complexity. The particular foundation system was then modelled by means of a simplified sub-structuring approach, considering separately the behaviour of the soil within the encasing ring (element 1 of Fig. 12) and of the soil below it (element 2); the two elements work in series, thus defining the global compressibility of the pier foundation. Element 1, owing to the presence of the encasing ring, was assumed to behave in a quasi-oedometric conditions, i.e. the horizontal displacement of the soil in this zone is almost inhibited by the presence of the encasing ring, and vertical strains only are developed. In favour of safety, moreover, the interface between the soil and the encasing ring was assumed to be perfectly smooth, i.e. the shear stress acting along the inner and outer sides of the ring are disregarded. Element 1 is in general expected to exhibit a marked locking effect, without the activation of any failure mechanism; from a

rheological point of view, its mechanical behaviour can be described by means of an overall vertical stiffness k_1.

The mechanical behaviour of element 2 was instead assimilated to that of a direct foundation, subjected to a lateral overburden given by the embedment of the encasing ring below the level of the riverbed. The deformability of this element can in principle be described by means of a generalized stiffness k_2, progressively reducing to zero during the tests (i.e. ductile response) until the final bearing capacity of the foundation is reached.

In the perspective of defining a preliminary predictive model, however, the values of k_1 and k_2 were considered constant (at least, limitedly to the loading levels prescribed by the testing program), and were calibrated according the procedure hereafter described.

6.1.3.1 Element 1

Given the limited valued of the applied load with respect to self-weight of each pier, the soil within element 1 is thought to behave in a small strain regime. Since no mechanical characterization at this strain level is available from the on-site campaign, an indirect strategy was then adopted, with reference to the experimental data published by Fioravante (2000) on seismic wave propagation in Ticino sand at similar relative density. By interpreting these results (Galli and Martinelli, 2016), a representative Young Modulus E = 240 MPa was estimated for the soil within the encasing rings. The corresponding values of the stiffness k_1 (depending on the area of the foundation and on the thickness of the soil layer within the rings) are reported in Table 3.

6.1.3.2 Element 2

The usual Brinch Hansen formula (Brinch Hansen, 1970) was employed to get a realistic estimation of the ultimate vertical bearing capacity R_m of element 2, thought as a direct foundation (the values are also listed in the Table 3); the obtained values are in all cases much larger than the test load, so that no global failure will be expected. It is however

fundamental to adopt a suitable modelling approach for describing the deformability of the foundation.

With respect to the linear elastic framework adopted for the predictive model, an equivalent secant stiffness was then iteratively estimated for element 2, by adopting the approach proposed by Berardi and Lancellotta (1991), which accounts the relative density D_R of the soil and the expected settlement level. An example of the load-settlement curve estimated for the piers 6, 7, 8, 9, and 10 is shown in Figure 14.

6.2 ULS model

The nonlinear FE model is based on the previous SLS model with three main changes with respect to what was described in Section 6.1:

a) the flexural stiffness of the RC slab is substituted with the flexural stiffness of the RC caisson;

b) the tensile strength of the arches is assumed equal to zero;

c) the soil behaviour is assumed to evolve according to the nonlinear soil-structure interaction model proposed by Nova and Montrasio (1991).

Regarding point c), the adopted model is a rigid-plastic generalized constitutive relationship with strain hardening and non-associated flow rule, capable of reproducing the response of a shallow foundations even to complex loading systems (i.e. vertical and horizontal forces, overturning moments). For the considered cases, however, only monotonic vertical loads are present, and the response is governed only by a parameter R_0 (function of the soil relative density D_R and representing the initial stiffness of the load-settlement curve) and by the vertical bearing capacity R_m (for further details, see Nova and Montrasio, 1991). One peculiarity of the Nova and Montrasio model is the capability of explicitly take into account the transition between a preloaded and a virgin

condition. If the applied load does not exceed the maximum load ever experienced by the foundation, the response of the system is reversible (i.e. linear elastic), and no significant permanent settlements are accumulated. In case the applied load exceeds the maximum value ever experienced, a virgin response is observed (i.e. elasto-plastic), with the accumulation of permanent settlement.

It results from historical data that in late 50's a heavy truck of about 90 tons (approximately 900 kN) went over the bridge; this load represents then an estimation of the maximum load ever experienced by the bridge. The ordinary traffic load is always well below such limit, meaning the foundation response is generally within the elastic regime. During the loading tests, however, the maximum load on each pier of approximately 1200 kN exceeded this limit thus potentially inducing permanent settlement in the foundation.

7 LOAD TEST RESULTS

7.1 Experimental vs numerical comparison

The experimental and numerical vertical settlement profile of the deck along the bridge axis for type A tests are shown in Figure 15. The vertical settlements shown in this figure are induced by the effect of the test load only. The type of test, the date and time of the test, the air temperature and the position and magnitude of the applied loads are indicated in the figure. It should be remembered that the final abbreviations "_1" and "_2" describe, respectively, a non-symmetrical and a symmetrical load scheme with respect to the keystone loaded arch. Negative displacement values indicate downward displacements.

In the transverse direction, the experimental reading points are located near the spandrel wall edges as shown in Figure 13. In the longitudinal direction the position of the experimental points is given in Figure 11. North and south experimental readings have

been mediated to be directly compared with numerical predictions, derived from a simple bi-dimensional model centred on the deck midway.

It is worth noting that the initial reference measurement of the bridge (zero-reading, without any applied load) was taken in a cloudy day condition, with an air temperature of 14.5 °C. All the type A tests were instead run in a sunny day condition, where a non negligible solar irradiation effect cannot a priori be foreseen. Unfortunately, this latter cannot be easily decomposed in the experimental readings from the mechanical part, which is the only component reproduced by the proposed numerical model.

The maximum experimental displacement recorded during type A tests is approximately 0.65 mm detected in test A7_2. This displacement is read at the keystone of arch 7 (which is considered to be the most significant, since it refers to the arch with the widest span). It is important to highlight that a suitable calibration of the whole model was carried out before the loading test, for the case of a truck with a weight equal to 320 kN used to inspect the bridge fronts and located in different points. The agreement between experimental and numerical results for the A7_2 test is very good, taking into account that the load considered in case An_2 is the double of that used for the calibration.

The thermal effect can largely justify the difference between numerical and experimental results visible in some tests (e.g. tests A4_2 and A8_2) and absent in others.

Figure 16 presents and discusses vertical settlement profiles for type B tests. In these tests, the thermal effect is virtually absent since the atmospheric condition during the loading phases was similar to that during the reference reading (unloaded bridge). The maximum experimental displacement of about 1.5 mm (of which about 1 mm accumulated from the foundation of the pier 6 and 0.7 mm from the foundation of the pier 7) was recorded during the B4 test by applying a load of about 1200 kN. This

displacement occurred at the keystone of arch 7.

Figure 16 also shows the difference between experimental readings carried out before and after the type B tests, with the aim of pointing out residual vertical settlements. The experimental reading of the residual settlement was carried out one day after from type B test. The maximum downward residual displacement induced by type B tests is approximately 0.4 mm (keystone of arch 7).

7.2 Prediction of ultimate bearing capacity

In this section, further numerical results obtained by means of the nonlinear FE model developed during the post-test phase are presented, with the aim of evaluating the bearing capacity of the bridge. The load scheme for the test B4 on arch 7 was considered as a reference.

A dimensionless loading parameter α, defined as

$$\alpha = \frac{P}{P_{exp}}, \tag{10}$$

is introduced, where P represents the applied load, normalized with respect to the maximum load P_{exp} = 1200 kN applied during the tests.

The numerical analysis was conducted up to a load level 3 times higher than the maximum load applied during the test (α = 3). The model labelled "1" in Figure 17 assumes hypotheses a) to c) introduced in Section 6.2, whilst model "2" removes the hypothesis b), thus pointing out the influence of the masonry nonlinearity with respect to model "1".

Figure 17a highlights how in both models nonlinearity affects the results since the very beginning (α < 0.5), but remarkable slope changes are observed at load levels of approximately $\alpha \cong 1.05$. These nonlinear effects are obviously induced by the soil

mechanical behaviour only. Evident differences between the two models are instead recognized only for $\alpha > 1.7$, meaning that after this point significant nonlinear effects are developing in the masonry too.

In Figure 17b the influence of the applied load on the internal state of stress in the bridge is finally presented. The results are expressed in terms of the maximum value of the principal compressive stress ($|\sigma_{III}|$) in the arches and in the piers, by varying the dimensionless loading parameter α. It is worth noting that the results corresponding to $\alpha = 0$ are representative of the internal state of stress generated by the bridge self-weight only. The curves of Figure 17b show that the internal state of stress in the piers is not remarkably modified by the applied load until the loading parameter α reaches approximately the value $\alpha = 0.6$, whilst in the arches significant modifications are observed only for load levels $\alpha > 1.7$.

In the perspective of providing a meaningful estimation of the bearing capacity of the whole bridge, by combining the results of Figures 17a and b, it can be concluded that for $\alpha < 0.6$ no significant modification in the internal state of stress in the bridge are induced by the applied load and the mechanical behaviour of the system lies within the linear regime (except for the soil). For $0.6 < \alpha < 1.7$ evident stress concentrations are observed in the piers, without inducing any nonlinearity in the masonry. Within this range, however, permanent vertical settlements of the bridge are observed, owing to the elasto-plastic behaviour of the soil.

Finally, for $\alpha > 1.7$, nonlinearity in the masonry mechanical behaviour plays a non-negligible role, and significant stress concentrations are observed in the arches too.

Given such considerations, for the proposed loading scheme, a loading value $\alpha=1.7$ can be assumed as a meaningful estimation of a representative bearing capacity of the

entire structure.

8 CONCLUSIONS

Over the course of almost seven centuries of life, the Azzone Visconti bridge has undergone profound changes related to different uses. The bridge has been transformed from a military fortress (protecting a strategic route of great commercial interest between the Duchy of Milan, the Republic of Venice and the preferred route to Northern Europe), to a major and unique way of communication between the towns of Milan and Lecco until 1955. Today the bridge keeps intact its immense historical value for the city of Lecco, but, from a technical point of view, it has to be considered as a bridge in II class use according to NTC08 (2008), with nominal life of 50 years.

Based on the extensive investigations ranging from three-dimensional geometric survey, to geotechnical and mechanical characterization of the materials, to experimental on-site tests, it is possible to derive the following conclusions.

The static tests carried out to estimate its bearing capacity allow to classify the bridge as a first class bridge, according to the provisions defined in NTC08 (2008). A total load of about 1200 kN was applied on the maximum span arch (arch 7, between the piers 6 and 7, clear span of 14.5 m) and a total settlement of about 1.5 mm at the keystone was measured. The foundation of the piers 6 and 7 have experienced a maximum settlement of about 1 mm and 0.7 mm, respectively. An irreversible vertical settlement of limited amplitude (~0.4 mm, about 30% of the total value) was recorded at the keystone of arch 7 at the end of the experimental test.

Based on the results of the experimental campaign, a simplified nonlinear two-dimensional structural model was defined, with the aim of investigating the bridge bearing capacity. The numerical tests were run for increasing values of the applied loads

P, normalized with respect to the maximum applied load P_{exp} in the experimental on-site tests ($\alpha = P/P_{exp}$). For $\alpha < 0.6$ no significant modifications in the internal state of stress of the bridge were induced with respect to that due to the bridge self-weight only.

For $0.6 < \alpha < 1.7$ evident stress concentrations are observed in the piers, and permanent vertical settlements of the bridge were observed (owing to the irreversible strains accumulated in the soil), but inducing negligible nonlinearities in the masonry.

For larger values of the applied load ($\alpha > 1.7$), significant stress concentrations were predicted in the arches too, and significant nonlinear effects (damage) could be induced in the masonry according to the performed analyses.

For the tested loading scheme, the value $\alpha = 1.7$ can be assumed as a meaningful estimation of a representative bearing capacity of the entire structure.

Given the historical significance of the bridge, and the will to preserve it well beyond the stated limit of nominal life (50 years), the authors believe that the passage of vehicles respecting the limit permitted by the road code (not exceeding the condition $\alpha = 0.6$) is surely a safe condition for the bridge. On the contrary, any type of exceptional transport should not be allowed.

ACKNOWLEDGEMETS

The Authors are in debt with the Municipality of Lecco and "Consorzio fiume Adda" for the precious historical and technical documents acquired with their help and Arch. Chiara Rostagno (official of Ministry of Cultural Heritage and Tourism, Superintendent of Fine Arts and Landscape) for the stimulating discussions and the appreciated suggestions on the historical material provided.

REFERENCES

Abaqus Analysis User's Manual. 2016. Version 6.14, vol. 2. Technical report, Simulia.

Bazaraa, A.R.S.S. 1967. The use of the standard penetration test for estimating settlements of shallow foundations on sand. PhD Thesis, University of Illinois.

Berardi, R., and Lancellotta, R. 1991. Stiffness of Granular soil from field performance. Geotechnique, 41(1):149–157.

Boothby, T. E. 2001. Load rating of masonry arch bridges. Journal of Bridge Engineering (ASCE), 6(2):79–86.

Brencich, A., De Francesco, U. 2004. Assessment of multi-span masonry arch bridges. Part I: A simplified approach. Part II: Examples and applications. Journal of Bridge Engineering (ASCE), 9(6):582–598.

Brinch Hansen, J. 1970. A revised and extended formula for bearing capacity. Bulletin n. 28, pp. 5-11. Copenhagen: Danish geotechnical Institute.

Bungey, J. H., Millard, S. G., and Grantham, M. G. 2006. Testing of concrete in structures. London: Taylor & Francis; Fourth Edition.

Cavicchi, A., and Gambarotta, L. 2005. Collapse analysis of masonry bridges taking into account arch-fill interaction. Engineering Structures, 27(4):605–615.

CEN 12390-3, 2009. Testing hardened concrete-Part 3: Compressive strength of test specimens. European Committee for Stand., Brussels.

CEN 12390-6, 2009. Testing hardened concrete-Part 6: Tensile splitting strength of test specimens. European Committee for Stand., Brussels.

de Felice, G. 2009. Assessment of the load-carrying capacity of multi–span masonry arch bridges using fibre beam elements. Engineering Structures, 31(8):1634–1647.

De Santis, S., and De Felice, G. 2014. Overview of railway masonry bridges with a safety factor estimate. International Journal of Architectural Heritage, 8(3):452–474.

di Prisco, C., and Galli, A. 2011. Mechanical behaviour of geo-encased sand columns: Small scale experimental tests and numerical modelling. Geomechanics and Geoengineering, 6(4):251–263.

Fanning, P. F., and Boothby, T. E. 2001. Three-dimensional modelling and full-scale testing of stone arch bridges. Computers & Structures, 79(29–30):2645–2662.

Fioravante, V. 2000. Anysotropy of small strain stiffness of Ticino and Kenya sands from seismic wave propagation measured in triaxial testing. Soils and Foundations, 40(4):129–142.

Galli, A., Martinelli, P. 2016. Experimental characterization and numerical investigation on the Azzone Visconti bridge in Lecco (Italy). Procedia Engineering 158:158–163.

Gibbs, H. J., Holtz, W. G. 1957. Research on determining the density of sand by spoon penetration test. Proc. 4th International Conference on Soil Mechanics and Foundation Engineering, 1:35–39.

Gilbert, M., and Melbourne, C. 1994. Rigid-block analysis of masonry structures. The Structural Engineer, 72(21):356–61.

Harvey, W. J. 1988. Application of the mechanism analysis to masonry arches. The Structural Engineer, 66(5):77–84.

Heyman, J. 1982. The masonry arch. London, UK: Ellis Horwood.

Lemos, J. V. 2007. Discrete element modelling of masonry structures. International Journal of Architectural Heritage, 1(2):190–213.

Lombardia Beni Culturali. Retrieved July 13, 2017, from http://www.lombardiabeniculturali.it

Magnani R. 2014. La Missione segreta di Leonardo da Vinci - Vol. 1 (in Italian).

Milani, G., and Lourenço, P. B. 2012. 3D non-linear behaviour of masonry arch bridges. Computers & Structures, 110–111:133–150.

Molins, C., and Roca, P. 1998. Capacity of masonry arches and spatial frames. Journal of Bridge Engineering (ASCE), 124(6):653–663.

Nova, R., and Montrasio, L. 1991. Settlements of Shallow Foundations on Sand. Geotechnique, 41(2):243–256.

NTC 2008. Nuove Norme Tecniche per le Costruzioni. Ministero delle Infrastrutture (GU n.29 04/02/2008), Rome, Italy; 14/01/2008 (in Italian).

O'Connor, C. 1994. Development in Roman stone arch bridges. Endeavour, New Series 18(4):158–163.

Pérez-Gracia, V., Di Capua, D., Caselles, O., Rial, F., Lorenzo, H., González-Drigo, R., and Armesto, J. 2011. Characterization of a romanesque bridge in Galicia (Spain). International Journal of Architectural Heritage, 5(3):251–263.

Schmertmann, J. H. 1976. Interpreting the dynamics of the SPT, Final Report on project D-636 to the Florida Department of Transposrtation, Research Division.

UK Department of Transport. 1997. Design manual for roads and bridges, vol. 3, sec. 4, part 4: The assessment of highway bridges and structures. London, UK: UK Department of Transport.

UNESCO World Heritage List. Retrieved July 28, 2017, from http://whc.unesco.org/en/list

Ural, A., Oruç, S., Dogangün, A., and Tulik, O. I. 2008. Turkish historical arch bridges and their deteriorations and failures. Engineering Failure Analysis, 15: 43–53.

LIST OF FIGURES

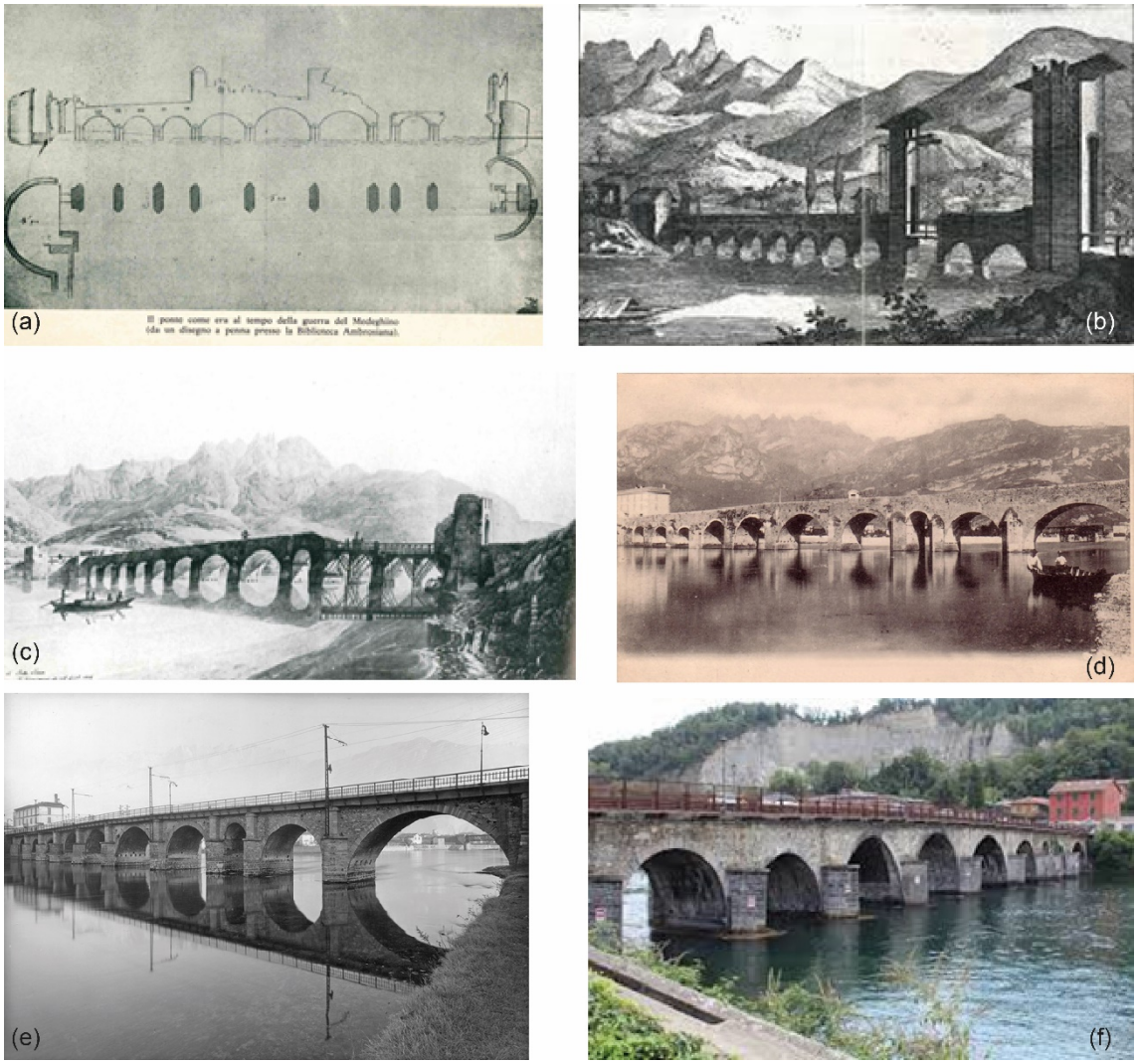

Fig. 1 (a-b) Plot of the bridge in the XVI century; (c) the bridge in 1806 (water-based paint by Peter Birmann) (d) view of the bridge at the beginning of XX century; (e) view of the bridge after the deck enlargement to host a tramway line and (f) view of the bridge in 2015. Courtesy of Lecco Municipality and "Soprintendenza belle arti e paesaggio".

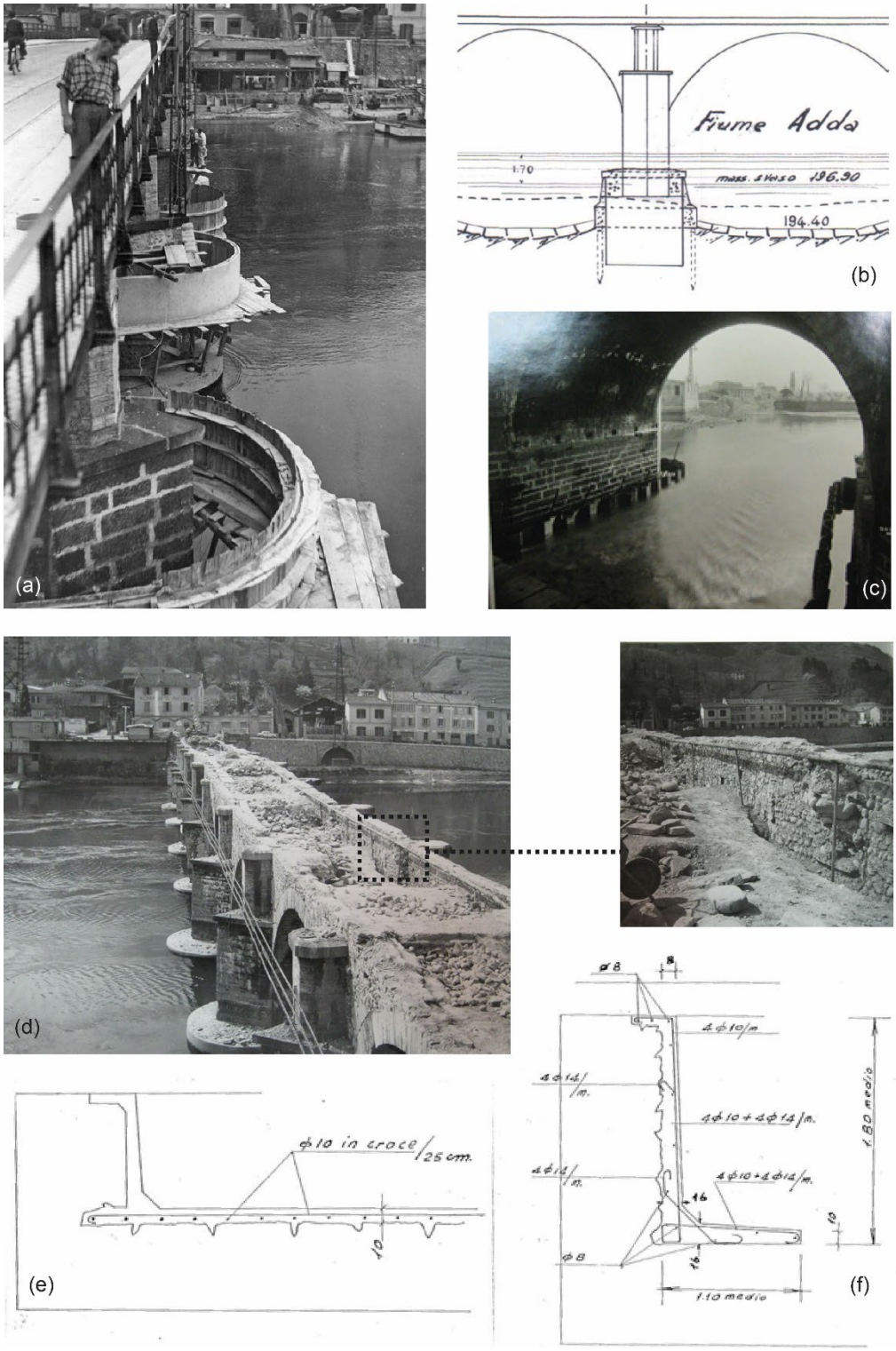

Fig. 2 (a-c) Strengthening works at the foundations in 1949-1950; (d-f) consolidation works in 1959-1960; (a-c) placement of the steel encasing ring and of the reinforcing concrete ring; (d) fill removal between spandrel walls and arches; (e) consolidation of the upper part of the arches and (f) consolidation of the spandrel walls. Courtesy of Lecco Municipality, "Consorzio Fiume Adda" and "Soprintendenza belle arti e paesaggio".

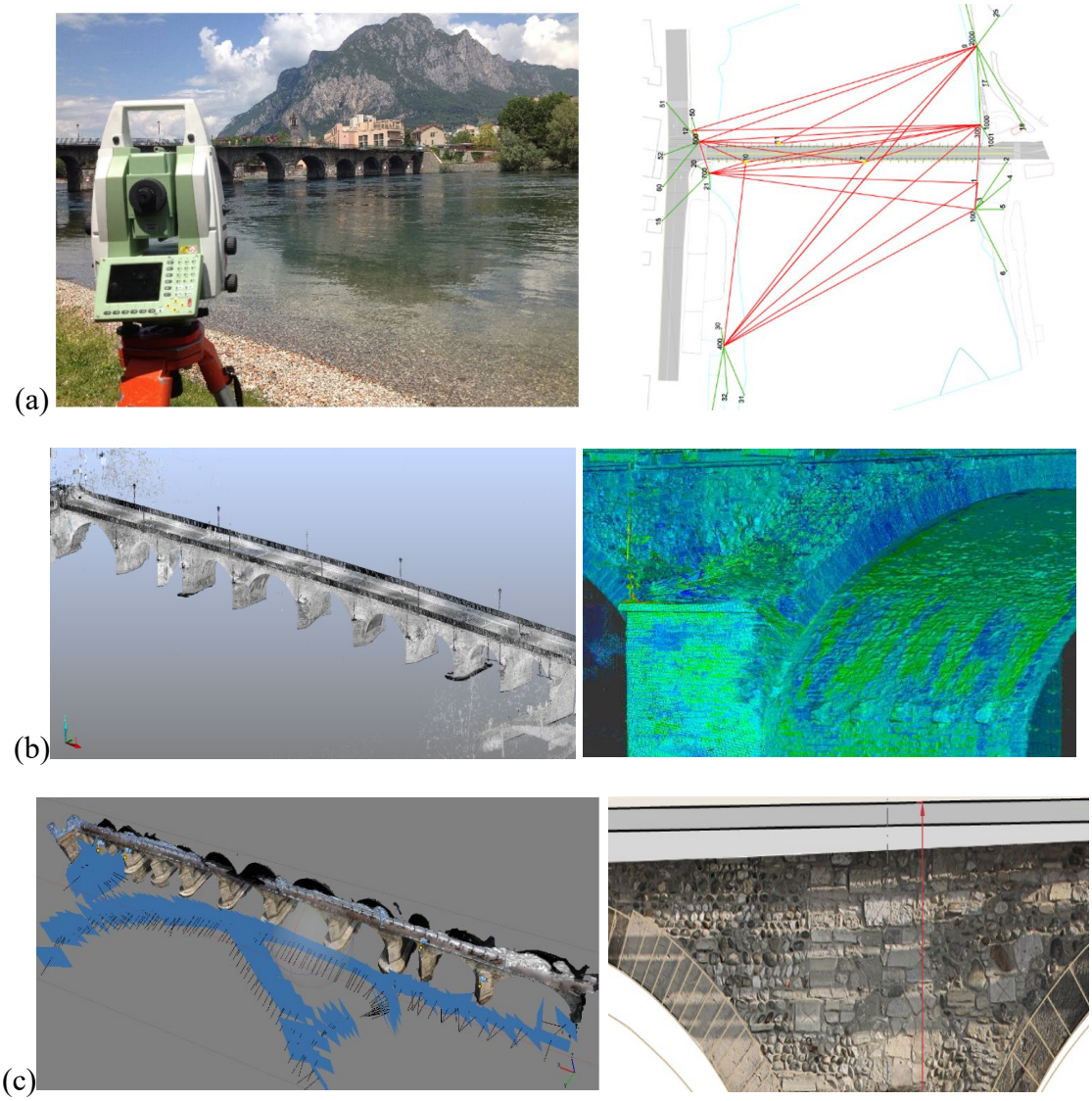

Fig. 3 The geometrical survey of the bridge: (a) the local geodetic network; (b) laser scanning survey: the overall bridge (left) and a detail of the intrados of a span (right) and (c) the photogrammetric survey of the bridge elevations: camera position (left) and a detail of the final orthophoto (right).

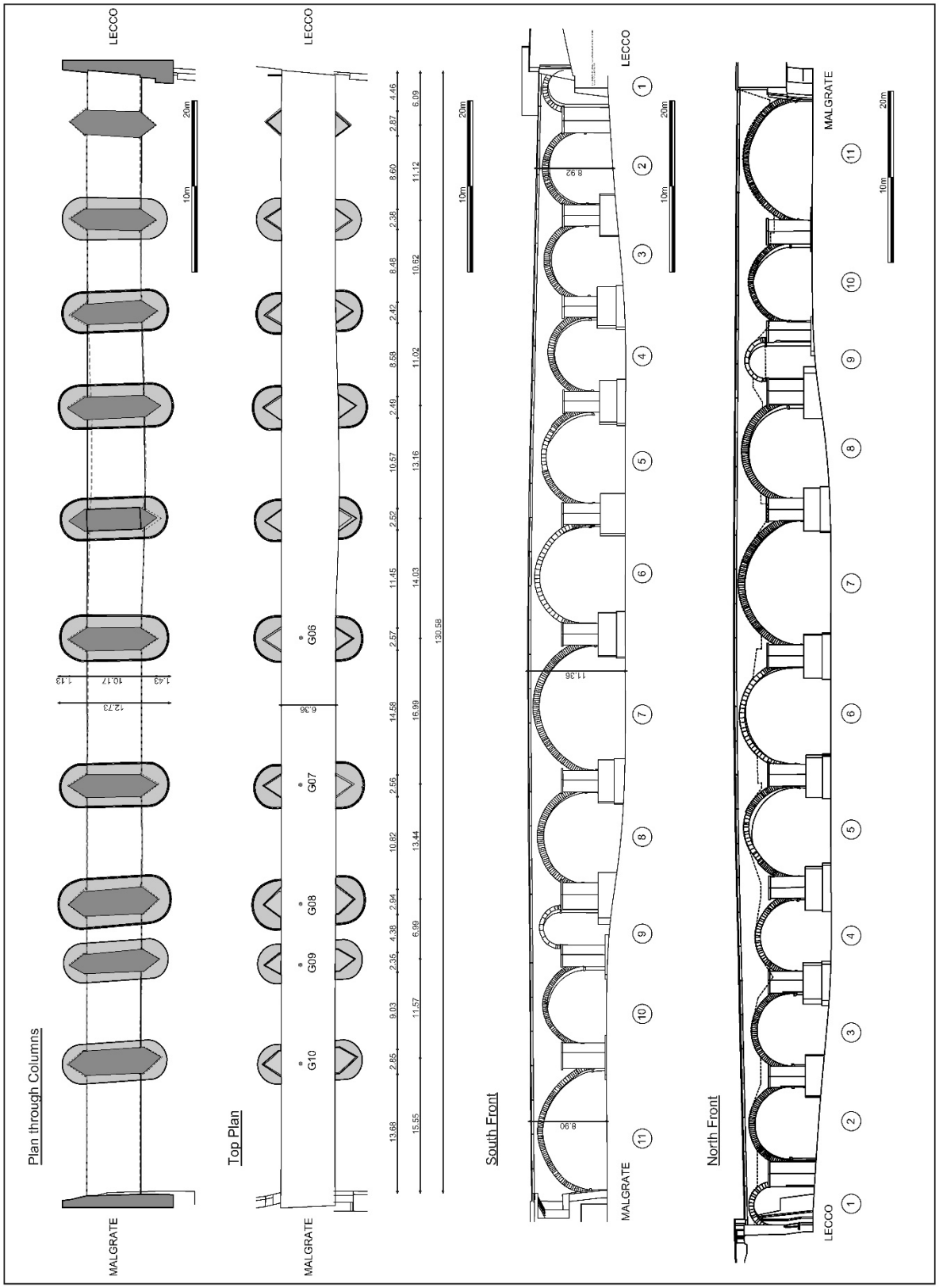

Fig. 4 Plan and front (downstream and upstream) views of the bridge.

(a) 

(b) 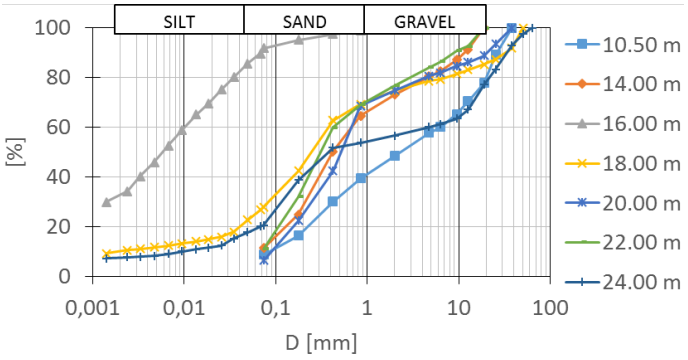

Fig. 5 (a) soil coring below pier 8, between 15 and 18 meters depth; (b) grain size distribution of the seven samples extracted below from core G08.

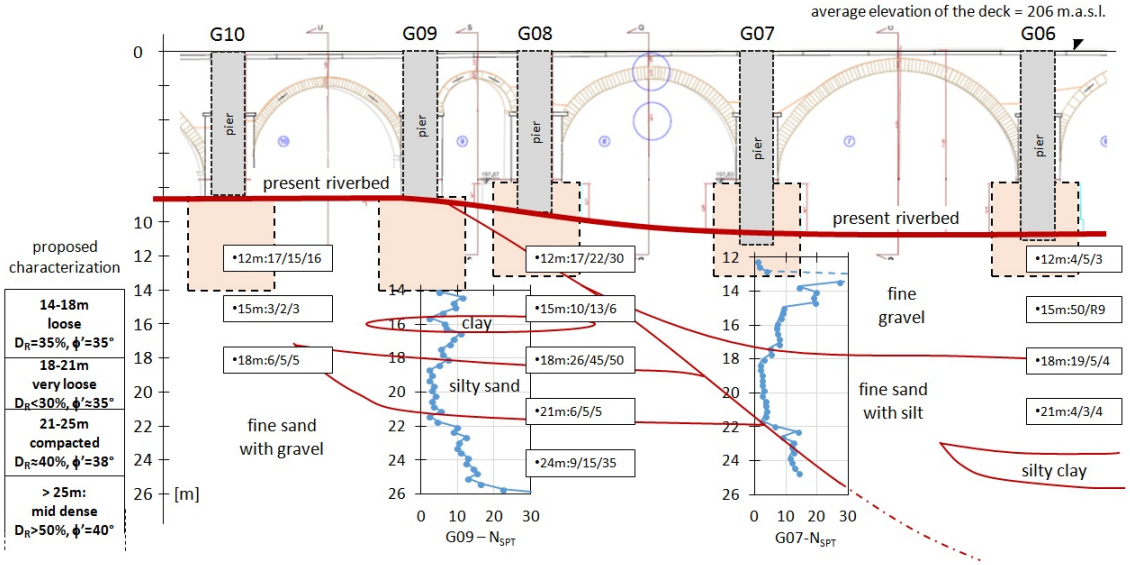

Fig. 6 Results of the SPT-DPSH tests performed below piers G07 and G09 and geotechnical model of the riverbed.

(a)

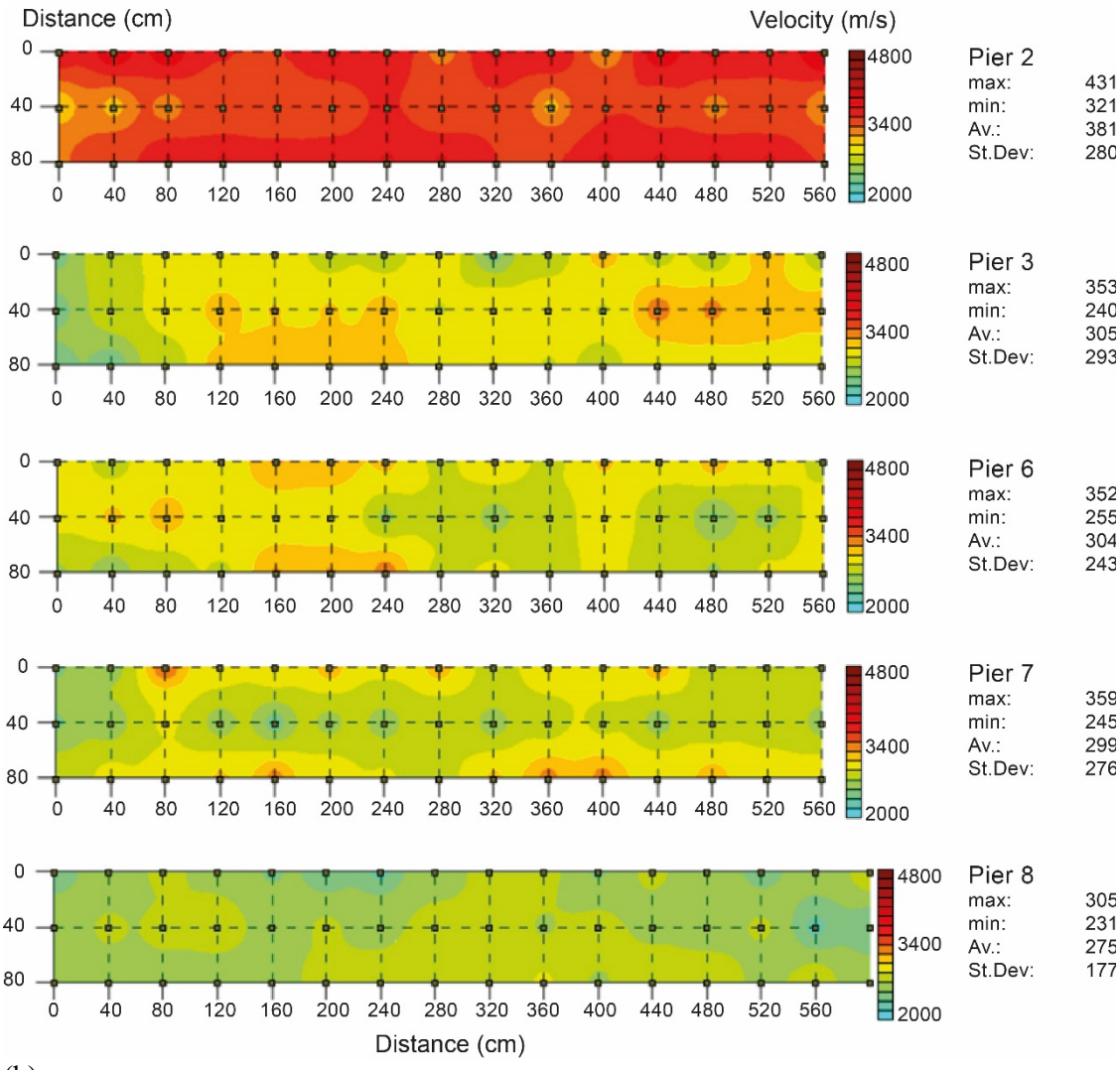

(b)

Fig. 7 Sonic test results: (a) superposition between the test area test results for pier 2 and (b) sonic surface graphs for piers 2, 3, 6, 7 and 8.

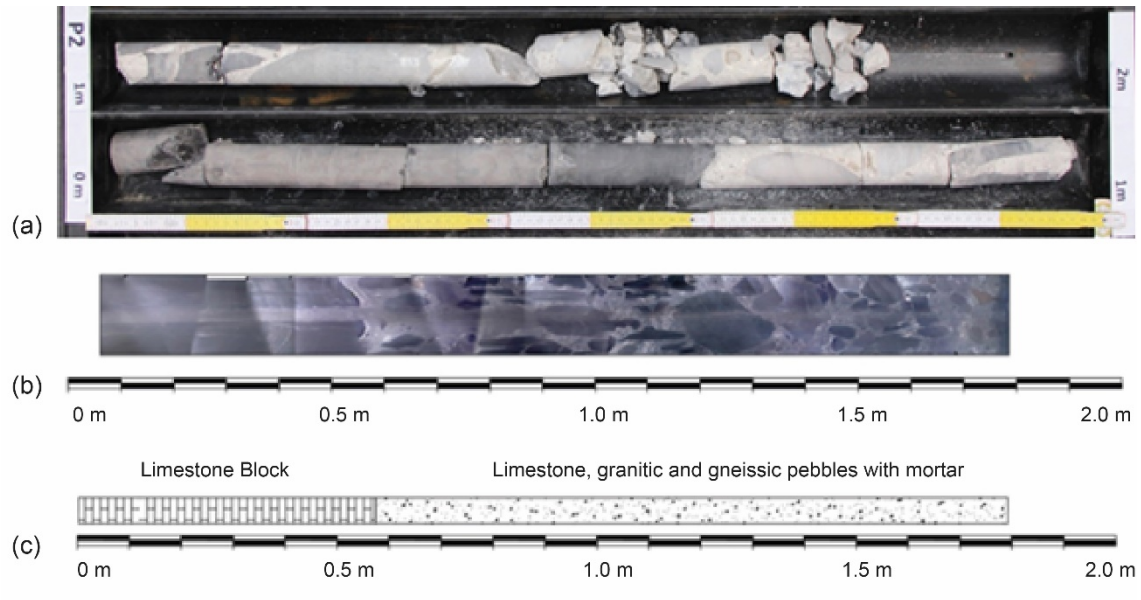

Fig. 8 (a) extracted core; (b) hole videoendoscopy (c) cross-section schematic return.

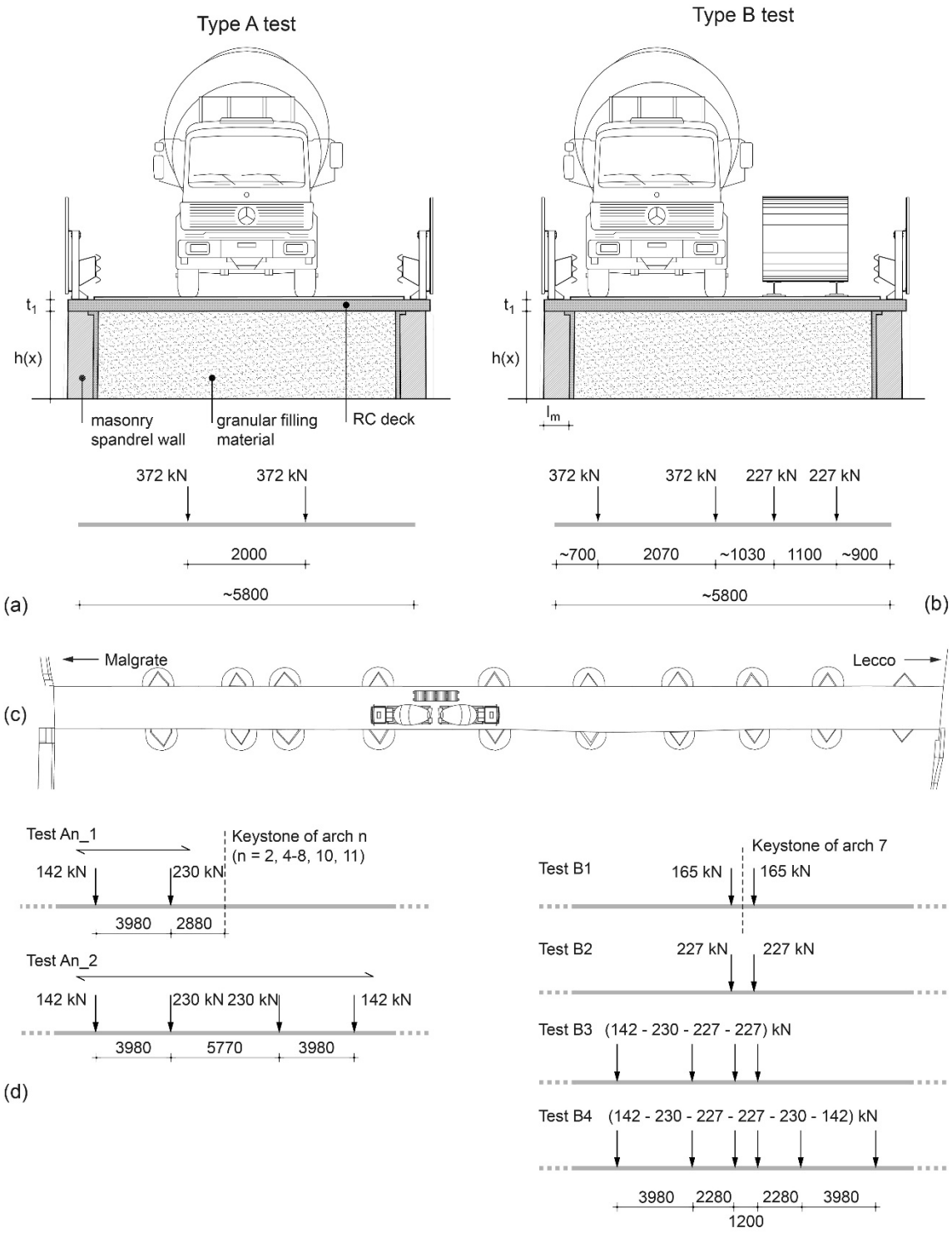

Fig. 9 Cross bridge view and load point identification for (a) type A and (b) type B tests, (c) plan view of the bridge: loading scheme type B4 and (d) longitudinal position for the load scheme adopted (lengths in mm).

Fig. 10 Load test type B: (a) positioning of 4 coils (phase B2); (b) positioning of 4 coils and one truck mixer (phase B3) and (c-d) positioning of 4 coils and two truck mixers (phase B4).

a.

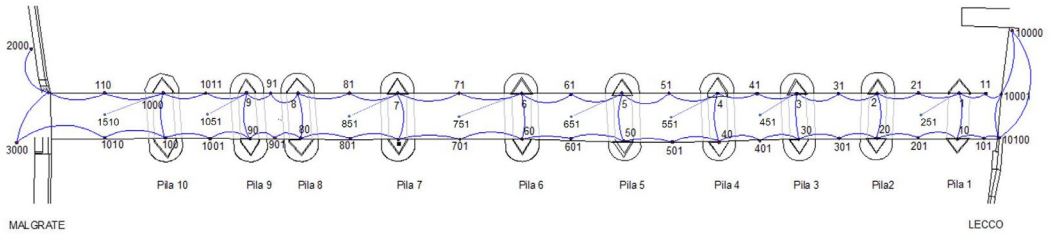

b.

Fig. 11 Displacement measurement during the loading tests: (a) levelling network scheme and (b) measurement phase.

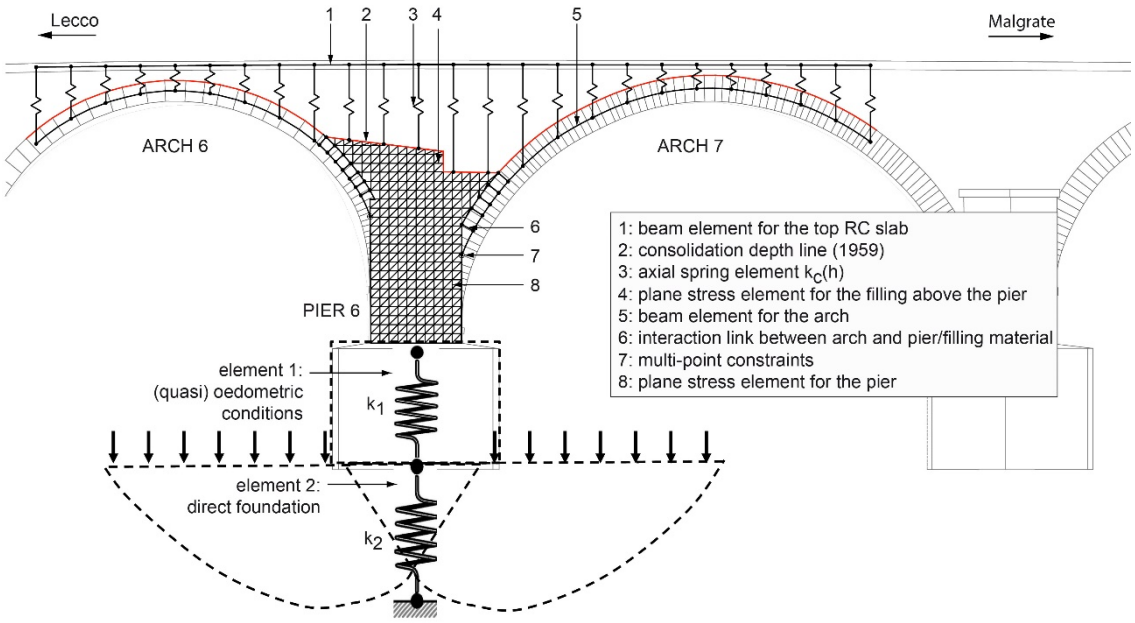

Fig. 12 Main components of FE model for the Azzone Visconti bridge.

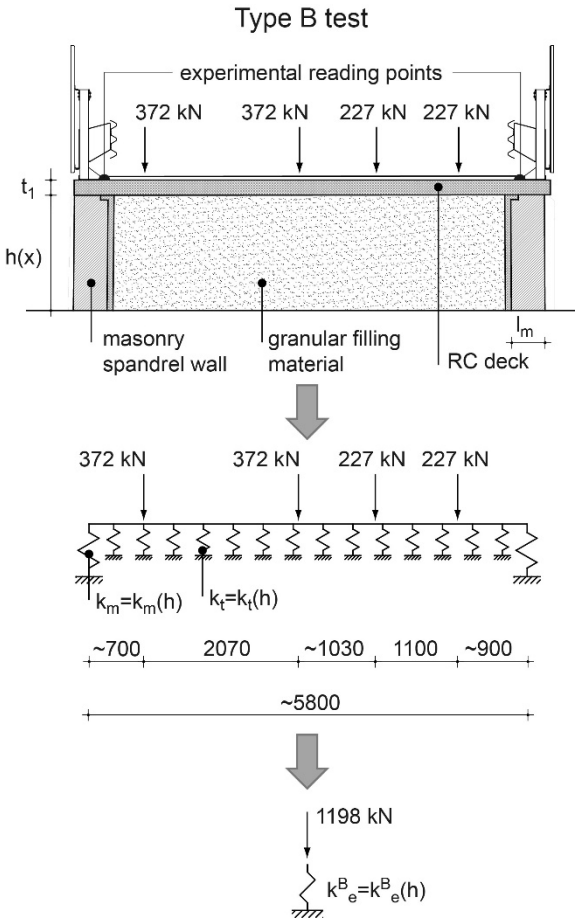

Fig. 13 Structural schemes adopted for the derivation of the vertical equivalent stiffness (length in mm; type B test)

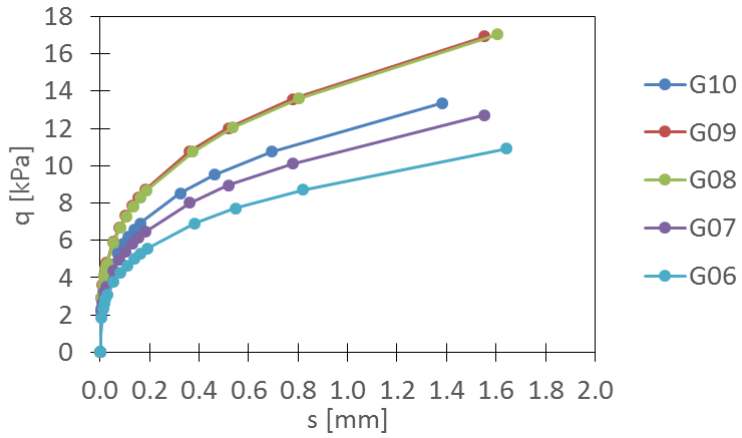

Fig. 14 Estimated load-settlement curve for element 2 according to Berardi and Lancellotta model for piers 6, 7, 8, 9 and 10.

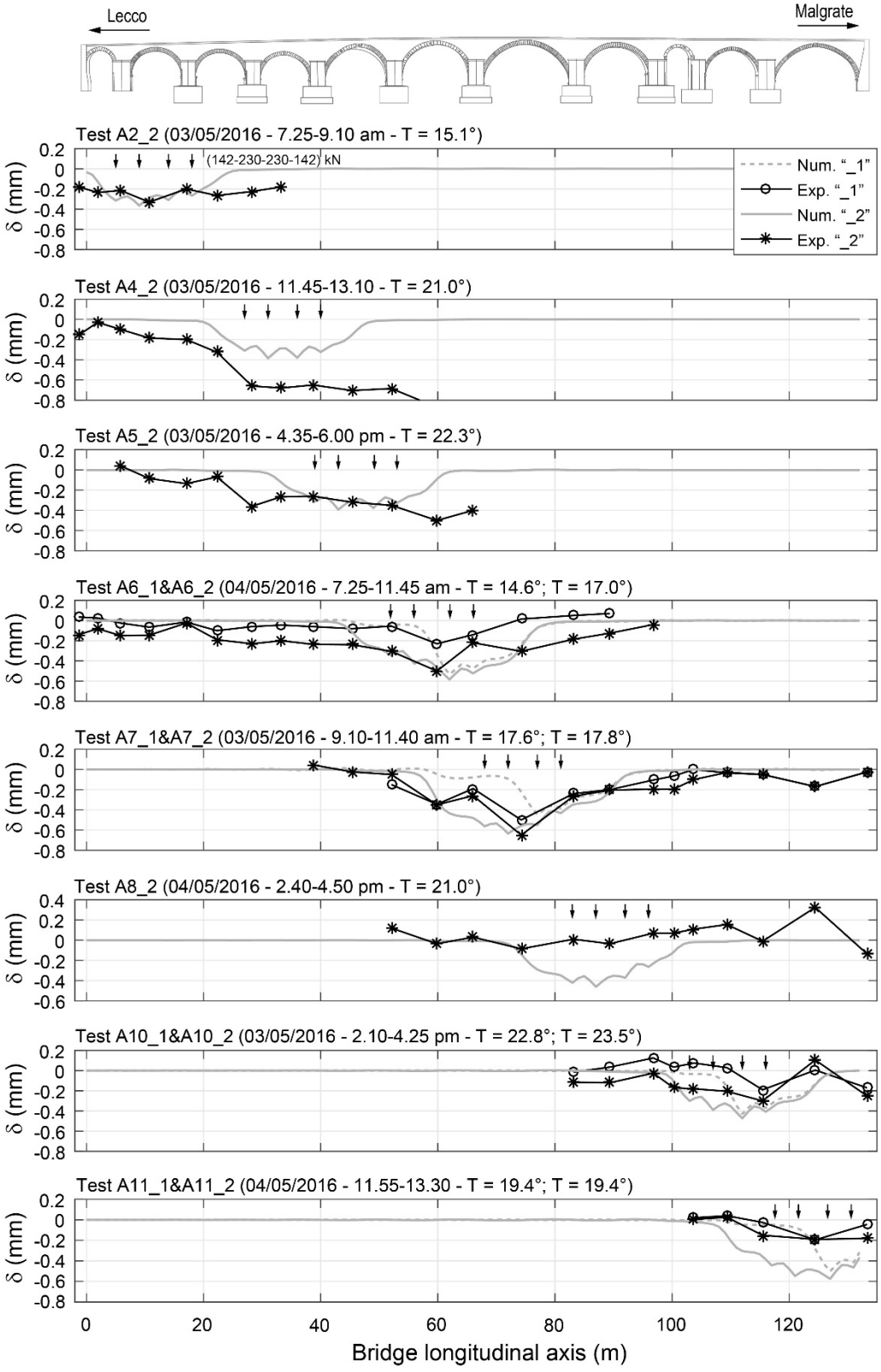

Fig. 15 Vertical settlements for type A tests: experimental and numerical results

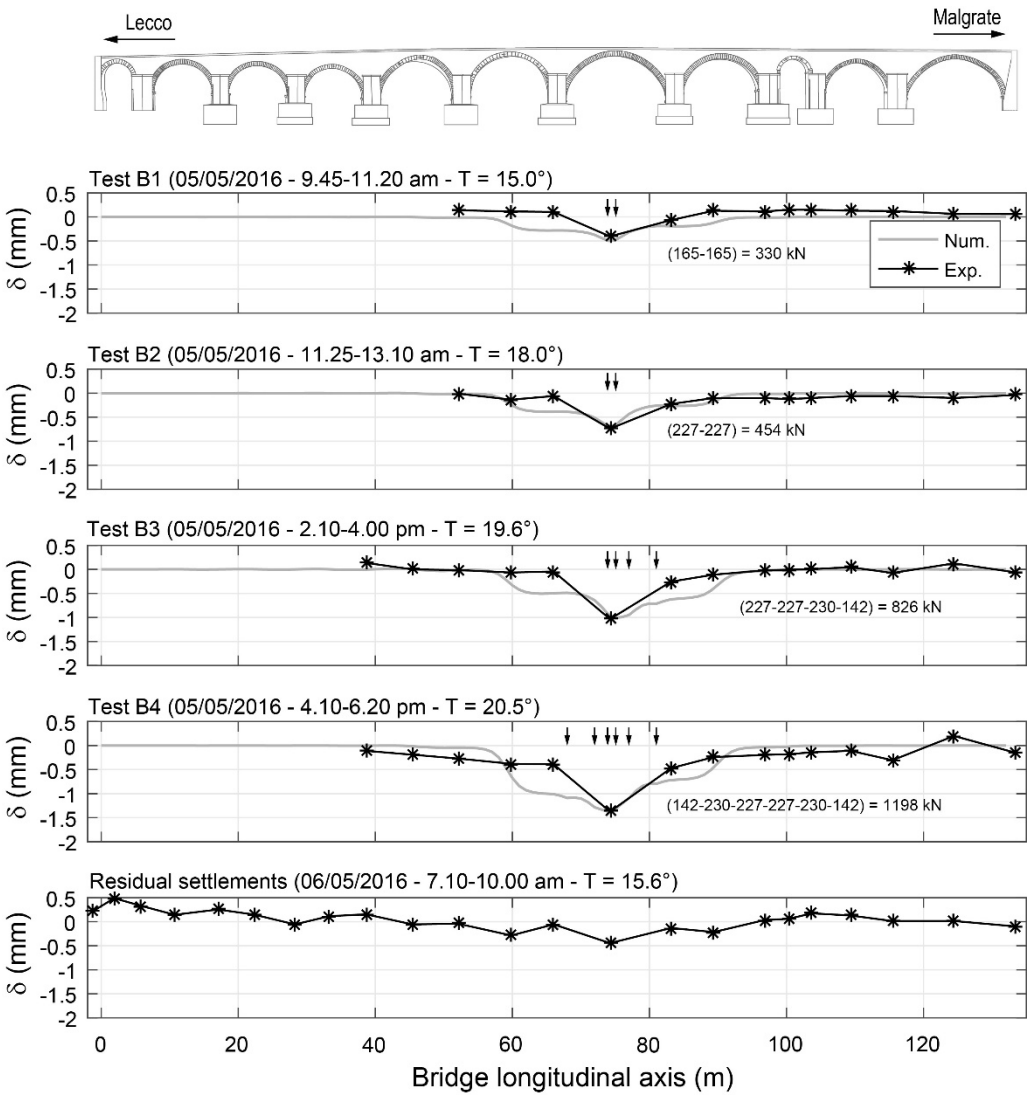

Fig. 16 Vertical settlements for type B tests: experimental and numerical results; residual vertical settlements recorded after type B tests

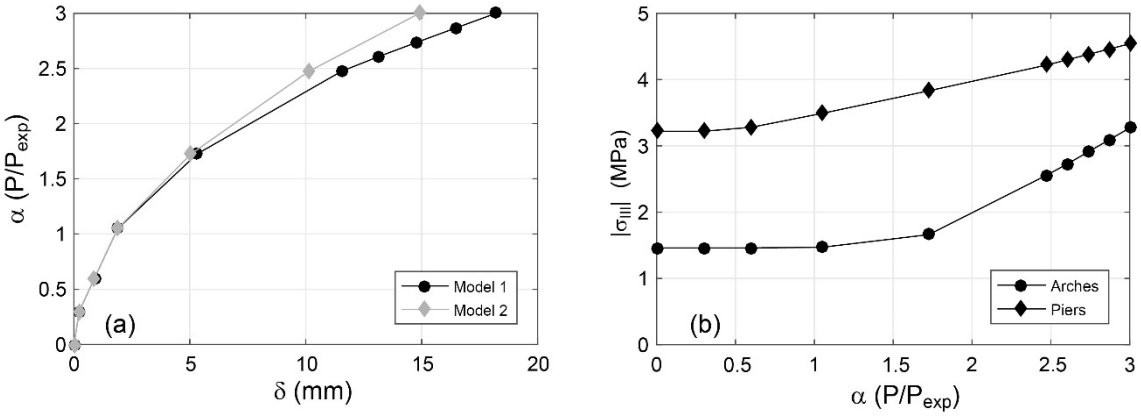

Fig. 17 Nonlinear finite element results: (a) numerical normalized load vs vertical displacements and (b) minimum principal stress in aches and piers as function of the normalized load

LIST OF TABLES

Test name	Loaded span	Load type
A2_2	2	2 truck mixers
A7_1	7	1 truck mixer
A7_2	7	2 truck mixers
A4_2	4	2 truck mixers
A8_2	8	2 truck mixers
A5_2	5	2 truck mixers
A10_1	10	1 truck mixer
A10_2	10	2 truck mixers
A6_1	6	1 truck mixer
A6_2	6	2 truck mixers
A11_1	11	1 truck mixer
A11_2	11	2 truck mixers
B1	7	2 coils
B2	7	4 coils
B3	7	4 coils + 1 truck mixer
B4	7	4 coils + 2 truck mixers

Table 1 Sequence of test types A and B

Bridge component	Density ρ (kg/m^3)	Young Modulus E (MPa)	Poisson coefficient (-)
Piers 1 and 2	2400	31350	0.2
Piers 3-7	2400	19860	0.2
Piers 8 and 9	2400	16400	0.2
Pier 10	2400	8200	0.2
Arches	2600	8000	0.2
RC top slab	2500	28500	0.2
Filling material	2000	-	-

Table 2 Mechanical characteristics and density for the different part of the bridge

	pier 6	pier 7	pier 8	pier 9	pier 10
k_l (MN/m)	7232.6	5860.9	4458.5	2972.7	2536.4
R_m (MN)	123.5	116.7	151.5	179.3	149.3

Table 3 Values of vertical stiffness k_l and bearing capacity R_m for piers 6 to 10.